TABLE OF CONTENTS

1. THEORY

1.1. Accelerating Charged Particles

1.1.1. Relation between momentum and acceleration

In classical mechanics, Newton's second law defines force and states

$$\vec{\mathbf{F}} = \frac{\partial \vec{\mathbf{p}}}{\partial t} = m\frac{\partial \vec{\mathbf{v}}}{\partial t} = m\vec{\mathbf{a}} \tag{1.1}$$

In special relativity however, relativistic momentum is defined as $\vec{p} = \gamma m_0 \vec{v}$ where γ is the Lorentz Factor;

$$\gamma = \frac{1}{\sqrt{1 - v^2/c^2}} = \frac{1}{\sqrt{1 - \beta^2}}$$

Considering these two statements, we can find the relation between momentum and acceleration as follows

$$
\begin{aligned}
\frac{\partial \vec{p}}{\partial t} &= m_0 \frac{\partial(\gamma\vec{v})}{\partial t} = m_0\{\frac{\partial\gamma}{\partial t}\vec{v} + \gamma\frac{\partial\vec{v}}{\partial t}\} \\
\frac{\partial\gamma}{\partial t} &= \gamma^3\vec{\beta}\cdot\frac{\partial\vec{\beta}}{\partial t} = \frac{\gamma^3}{c}\vec{\beta}\cdot\vec{a} \\
\frac{\partial\vec{p}}{\partial t} &= m_0\{\frac{\gamma^3}{c}(\vec{\beta}\cdot\vec{a})\vec{v} + \gamma\frac{\partial\vec{v}}{\partial t}\}
\end{aligned}
$$

$$\vec{\mathbf{F}} = \gamma m_0\{\vec{\mathbf{a}} + \gamma^2(\vec{\beta}\cdot\vec{\mathbf{a}})\vec{\beta}\} \tag{1.2}$$

It is clear that acceleration is not necessarily parallel to the force anymore.

To start seperating the parallel and perpendicular components relative to $\vec{\beta}$, we

can find $\vec{\mathbf{a}}_{||}$ and $\vec{\mathbf{F}}_{||}$.

$$\vec{\mathbf{a}}_{||} = \frac{(\vec{a} \cdot \vec{\beta})}{\beta^2}\beta \qquad\qquad \vec{\mathbf{F}}_{||} = \frac{(\vec{F} \cdot \vec{\beta})}{\beta^2}\beta \qquad\qquad (1.3)$$

$$\begin{aligned} \vec{\mathbf{F}} \cdot \vec{\beta} &= \gamma m_0\{\vec{\mathbf{a}} \cdot \vec{\beta} + \gamma^2(\vec{\beta} \cdot \vec{\mathbf{a}})\beta^2\} \\ &= \gamma m_0(\vec{\mathbf{a}} \cdot \vec{\beta})\{\gamma^2\beta^2 + 1\} \end{aligned}$$

Using $\gamma^2\beta^2 + 1 = \gamma^2$ we have,

$$\vec{\mathbf{F}} \cdot \vec{\beta} = m_0\gamma^3(\vec{\mathbf{a}} \cdot \vec{\beta})$$

Inserting this

$$\begin{aligned} \vec{\mathbf{F}}_{||} &= \frac{(\vec{\mathbf{F}} \cdot \vec{\beta})}{\beta^2}\vec{\beta} \\ &= m_0\gamma^3\frac{(\vec{\mathbf{a}} \cdot \vec{\beta})}{\beta^2}\vec{\beta} \\ &= m_0\gamma^3\vec{\mathbf{a}}_{||} \qquad\qquad (1.4) \end{aligned}$$

Therefore from *equations 1.2 and 1.4*

$$\begin{aligned} \vec{\mathbf{F}} &= m_0\gamma^3\vec{\mathbf{a}}_{||}\beta^2 + m_0\gamma\vec{\mathbf{a}} \\ &= m_0\gamma^3\vec{\mathbf{a}}_{||}\beta^2 + m_0\gamma\{\vec{\mathbf{a}}_{||} + \vec{\mathbf{a}}_{\perp}\} \\ &= m_0\vec{\mathbf{a}}_{||}\gamma\{\gamma^2\beta^2 + 1\} + m_0\gamma\vec{\mathbf{a}}_{\perp} \\ &= m_0\vec{\mathbf{a}}_{||}\gamma^3 + m_0\gamma\vec{\mathbf{a}}_{\perp} \\ &= \vec{\mathbf{F}}_{||} + m_0\gamma\vec{\mathbf{a}}_{\perp} \end{aligned}$$

We finally have two seperate equations which are in similar form with *equation 1.1.*

$$\vec{\mathbf{F}}_{||} = \gamma^3 m_0\vec{\mathbf{a}}_{||} \qquad\qquad \vec{\mathbf{F}}_{\perp} = \gamma m_0\vec{\mathbf{a}}_{\perp} \qquad\qquad (1.5)$$

1.1.2. Lorentz Force

Force acting on a charged particle moving in electromagnetic fields is called Lorentz Force and is given by the formula

$$\frac{\partial \vec{p}}{\partial t} = \vec{F}_L = q(\vec{E} + \vec{v} \times \vec{B})$$

(1.6)

where the q is the charge and $\vec{v}$ is the velocity of the particle.

1.1.3. Relativistic Lorentz Force

Similar to non-relativistic version, relativistic Lorentz Force is given by the following 4-vector equality

$$\frac{\partial p^{\mu}}{\partial \tau} = qF^{\mu\nu}u_{\nu}$$

(1.7)

Where $\partial \tau = \partial t / \gamma$,

$$p^{\mu} = \begin{bmatrix} W/c \\ p_x \\ p_y \\ p_z \end{bmatrix} \qquad F^{\mu\nu} = \begin{bmatrix} 0 & -E_x/c & -E_y/c & -E_z/c \\ E_x/c & 0 & -B_z & B_y \\ E_y/c & B_z & 0 & -B_x \\ E_z/c & -B_y & B_x & 0 \end{bmatrix} \qquad u_{\nu} = \gamma \begin{bmatrix} c \\ -v_x \\ -v_y \\ -v_z \end{bmatrix}$$

(1.8)

Where W is the energy of the particle and γ is the lorentz factor mentioned in the previous section.

For $\mu = 0$, we have the time component of the equation;

$$\frac{\gamma}{c}\frac{\partial W}{\partial t} = \frac{q\gamma \vec{E}\cdot\vec{v}}{c} = \frac{q\gamma}{c}\frac{\vec{E}\cdot\partial\vec{r}}{\partial t} \tag{1.9}$$

$$\frac{\partial W}{\partial t} = q\frac{\vec{E}\cdot\partial\vec{r}}{\partial t} \tag{1.10}$$

This is the definition of work done by an electric field. For $\mu = 1, 2, 3$, we have the spacial components;

$$\frac{\partial\vec{p}}{\partial\tau} = \gamma\frac{\partial\vec{p}}{\partial t} = q\gamma(\vec{E} + \vec{v}\times\vec{B})$$

Which simplifies to non-relativistic Lorentz Force in *equation 1.6*.

1.1.4. Acceleration caused by lorentz force

Due to the nature of the cross product, lorentz force caused by a magnetic field is always perpendicular to the velocity of the particle. Therefore the acceleration of the magnetic field is straightforward

$$\vec{F}_B = \vec{F}_\perp = \gamma m_0 \vec{a}_\perp = \gamma m_0 \vec{a}_B$$

The same thing cannot be said about electric field however. It can create force in any direction with respect to velocity. Therefore, we have the following equality;

$$\vec{a}_\parallel = \frac{q}{\gamma^3 m_0}\vec{E}_\parallel \qquad \vec{a}_\perp = \frac{q}{\gamma m_0}\{\vec{E}_\perp + \vec{v}\times\vec{B}\} \tag{1.11}$$

Acceleration due to electric field can be simplified as;

$$\begin{aligned}
\vec{a}_{\{B=0\}} = \vec{a}_E &= \vec{a}_\parallel + \vec{a}_{\perp\{B=0\}} \\
&= \frac{q}{m_0\gamma}\{\frac{\vec{E}_\parallel}{\gamma^2} + \vec{E}_\perp\} \\
&= \frac{q}{m_0\gamma}\{\{1 - \beta^2\}\vec{E}_\parallel + \vec{E}_\perp\}
\end{aligned}$$

$$= \frac{q}{m_0\gamma}\{\vec{\mathbf{E}}_{||} + \vec{\mathbf{E}}_\perp - \beta^2\vec{\mathbf{E}}_{||}\}$$

$$= \frac{q}{m_0\gamma}\{\vec{\mathbf{E}} - \beta^2\vec{\mathbf{E}}_{||}\}$$

Using the fact that $\vec{\mathbf{E}}_{||} = \vec{\beta}(\vec{\mathbf{E}}\cdot\vec{\beta})/\beta^2$, we finally have

$$\vec{\mathbf{a}}_E = \frac{q}{\gamma m_0}\{\vec{\mathbf{E}} - \vec{\mathbf{v}}\frac{(\vec{\mathbf{E}}\cdot\vec{\mathbf{v}})}{c^2}\} \qquad \vec{\mathbf{a}}_B = \frac{q}{\gamma m_0}(\vec{\mathbf{v}}\times\vec{\mathbf{B}}) \qquad (1.12)$$

1.2. Particle Accelerators

Particle accelerators are sophisticated scientific instruments designed to accelerate charged particles, such as electrons, protons, or ions, to high speeds and energies. These accelerators play a crucial role in advancing our understanding of the fundamental properties of matter and the universe. They are widely used in various fields of research, including particle physics, nuclear physics, materials science, and medicine.

At their core, particle accelerators utilize electromagnetic fields to impart energy to particles and control their trajectories. These fields are generated by intricate arrangements of magnets and RF (radiofrequency) cavities within the accelerator structure. By precisely controlling these fields, accelerators can propel particles to speeds close to the speed of light, enabling them to acquire high energies.

Accelerators can be categorized into two main types: linear accelerators (linacs) and circular accelerators. Linacs accelerate particles in a straight line, while circular accelerators use magnetic fields to bend the particle trajectory into a circular path.

The acceleration process in accelerators involves multiple stages. Initially, particles are injected into the accelerator at a relatively low energy. As they progress through the accelerator, they are subjected to alternating electric fields that accelerate them, while magnetic fields guide their trajectories. Focusing elements, such as magnetic lenses or quadrupole magnets, ensure the particles remain tightly controlled.

As particles gain energy in the accelerator, they approach relativistic speeds, where relativistic effects become significant. Special relativity governs the increase in mass and energy of the particles as they approach the speed of light, providing insights into the behavior of matter at high energies.

Particle accelerators are essential tools for scientific research. They enable scientists to probe the fundamental constituents of matter, study particle interactions, and

explore the laws of physics. Accelerators have been instrumental in discovering and characterizing fundamental particles, such as quarks, leptons, and the Higgs boson. They also facilitate the production of high-intensity beams for applications in material science, radiotherapy, and industrial processes like particle irradiation and sterilization.

Figure 1.1: A circular accelerator

Figure 1.2: A linear accelerator

1.2.1. Key Concepts

- Phase Stability
- Phase Lag
- Shunt Impedance

1.2.2. Acceleration Cavities

Radiofrequency (RF) cavities, also known as accelerating cavities or resonant cavities, are key components in particle accelerators. These cavities generate strong electromagnetic fields at specific frequencies to accelerate charged particles through clever engineering.

RF cavities are typically hollow metallic structures made of or coated with high-conductivity materials such as copper. They are designed to resonate at a specific frequency, which is determined by the size and shape of the cavity. The cavity is often cylindrical or spherical in shape, and its inner surface is polished to minimize energy losses through resistive heating. The RF cavity is designed to be resonant, meaning that it naturally amplifies the electric fields at its resonant frequency. The resonant frequency is determined by the cavity's dimensions and the speed of light in the cavity material.

To achieve efficient energy transfer to the particles, the RF cavity is driven by an external RF power source operating at the resonant frequency. The power source supplies radiofrequency energy to the cavity, which causes the electric fields inside the cavity to oscillate at the desired frequency. These oscillating fields then transfer energy to the passing particles, increasing their kinetic energy by pushing and pulling on the charged particles as they pass through the cavity.

In addition to accelerating the particles, RF cavities are often designed to provide focusing forces. By carefully shaping the cavity and adjusting the electromagnetic fields, the particles can experience focusing effects as they pass through the cavity. This helps to maintain a tight and controlled beam. To ensure efficient acceleration, it is essential to maintain phase stability. This means that the particles should experience the strongest electric fields at the correct time during their passage through the cavity. Precise timing and synchronization of the RF power source with the particle beam are crucial to achieve phase stability and maximize energy transfer.

Image Coming Soon

Figure 1.3: A rf cavity used in KAHVELab

1.2.3. Steerer Magnets

Steerer magnets, also known as dipole magnets or bending magnets, are fundamental components used in particle accelerators to control the trajectory of charged particles. They utilize the Ampere's Law to exert a magnetic field that interacts with the charged particles in the accelerator.

According to the Lorentz Force Law (*Section 1.1.2*), when a charged particle moves through a magnetic field, it experiences a force perpendicular to both its velocity vector and the magnetic field direction. This force causes the particle's trajectory to curve, resulting in a bending effect.

Image Coming Soon

Figure 1.4: A steerer magnet used in KAHVELab

1.2.4. Rhodotron Accelerator

Rhodotron Accelerator is a type of particle accelerator that was proposed by *Jacques POTTIER* in his publication *A new type of rf electron accelerator:The Rhodotron* in 1989 [1]. First prototype was built at CEA Saclay later in 1992 [2]. Its named after the greek word for rose, *rhodos*, due to the shape of the design [3].

The design of a rhodotron mainly consists of a coaxial cylindrical RF cavity and steerer magnets surrounding it. RF cavity is fed by an external RF source, accelerating the electrons entering from an attached electron gun.

1.2.4.1. Cavity of a Rhodotron. Coaxial design of the cavity concentrates the electric field, while the magnetic field diminishes in the middle of the cylinders. Therefore the electrons are injected and accelerated in the plane of zero magnetic field where the electric field is strongest.

Figure 1.5: SUPERFISH simulation of a coaxial cavity

Image Coming Soon

Figure 1.6: CST simulation of a coaxial cavity

With the expectation that the electrons will accelerate to speeds $>= 0.9c$ after the first pass, a rhodotron cavity is designed so that the length of the path between successive passes is an integer multiple of λ, wavelength of the RF field ($l = p\lambda$). This constraint helps with phase stability and synchronization of the beam.

In the table below, optimized characteristics of a rhodotron cavity can be observed.

Table 1
Optimized characteristics

P	R_2 (m)	R_1/R_2	Z_{se} (MΩ)	Z_{sp} (MΩ)
1	0.27λ	$1/4$	$5.77\lambda^{1/2}$	$4.9\lambda^{1/2}$
2	0.5λ	$1/7$	$10.4\lambda^{1/2}$	$8.83\lambda^{1/2}$

Figure 1.7: Optimized characteristics of a rhodotron cavity [1]

Here, p is the integer multiplier in the equation ($l = p\lambda$) mentioned above, R_1 is the radius of the inner cylinder, R_2 is the radius of the outer cylinder, Z_{se} is effective shunt empedance, Z_{sp} is practical shunt empedance which was taken to be $0.85Z_{se}$.

Energy gain after each pass can be calculated by the following formula [1]

$$W_1 = Z_{sp}^{1/2} P^{1/2} cos\phi \tag{1.13}$$

Where P is the dissipated power, ϕ is the phase lag, taken as 15° [1].

Considering $Z_{sp} \propto \lambda^{1/2}$, $\quad W_1 \propto \lambda^{1/4}$, $\quad V \propto \lambda^3$, where V is the volume of the cavity, implementing the $p = 1$ design in *figure 1.7* is much more space efficient.

Table 2

Energy W (MeV) for $P = 100$ kW and $f = 130$ MHz

R_2 (m)	2	3	4	5	6	7	8	9	10	11	12
0.62	1.8	2.7	3.6	4.5	5.4	6.3	7.2	8.1	9	9.9	10.8
1.15	2.4	3.6	4.8	6	7.2	8.4	9.6	10.8	12	13.2	14.4

Figure 1.8: Energy of a synchronous electron after each pass for both $p = 1$ and $p = 2$ [1]

Total energy gain after n passes W can then be found by *equation 1.13*, taking $\phi = 15°$, $p = 1$, i.e $R_2 = 0.27\lambda$.

$$W \approx 2.14\lambda^{1/4} P^{1/2} n \quad keV \tag{1.14}$$

1.2.4.2. Acceleration cycle of Rhodotron. Electrons undergo four different stages during a single pass. They are accelerated between the cylinderical plates and are shielded from the changing RF field while inside the inner cylinder and outside the cavity.

First acceleration Electrons in the rhodotron cavity are accelerated by the electric

field created between two coaxial cylinders, towards the inner cylinder when they are ejected into the cavity.

Inner shielding While inside the inner cylinder, the cylinder acts as a faraday cage and shields the electrons inside while the electric field is being reversed.

Second acceleration Once the electrons leave the inner cylinder, they accelerate towards the outer cylinder by the reversed electric field until they leave the cavity.

Magnets After leaving the cavity, an electromagnet placed in their path steers the electrons back into the cavity in which time the electric field changes the direction again.

This cycle can be repeated as long as real world constraints such as; placements and dimentions of the electromagnets, power requirements due to increasing magnetic field in order for sharper turns, can be overcomed. After desired amount of pass has been completed, the electrons exit the accelerator.

This process is explained further in the following figures where T is the period of the electric field.

Figure 1.9: $[0, \frac{T}{4}]$ time frame of a rhodotron

Figure 1.10: $[\frac{T}{4}, \frac{T}{2}]$ time frame of a rhodotron

Figure 1.11: $[\frac{T}{2}, \frac{3T}{4}]$ time frame of a rhodotron

Figure 1.12: $[\frac{3T}{4}, T]$ time frame of a rhodotron

1.3. Numerical Integration Methods

1.3.1. Leapfrog

The Leapfrog method is a numerical method commonly used to solve ordinary differential equations (ODEs) that involve second-order time derivatives. Such an ODE is shown below:

$$\ddot{x} = \frac{d^2x}{dt^2} = f(x) \tag{1.15}$$

The Leapfrog method is a variant of the finite difference method, and it approximates the solution of an ODE by discretizing both time and space. The method gets its name from the way it calculates the values of the solution at each time step, which resembles a "leapfrogging" motion. It is a simple and efficient algorithm that is often used in simulations of physical systems, such as celestial mechanics or molecular dynamics. The idea is straight forward; in the time interval Δt,

$$
\begin{aligned}
a(t_0) &= f(x_0) \\
x(t_0 + \Delta t) &= x(t_0) + v(t_0)\Delta t + a(t_0)\frac{\Delta t^2}{2} \\
v(t_0 + \Delta t) &= v(t_0) + \{a(t_0) + a(t_0 + \Delta t)\}\frac{\Delta t}{2}
\end{aligned}
\tag{1.16}
\tag{1.17}
$$

For more stability, this version can be rearranged to what is called 'kick-drift-kick' form,

$$
\begin{aligned}
v(t_0 + \Delta t/2) &= v(t_0) + a(t_0)\frac{\Delta t}{2} \\
x(t_0 + \Delta t) &= x(t_0) + v(t_0 + \Delta t/2)\Delta t
\end{aligned}
\tag{1.18}
$$

$$v(t_0 + \Delta t) \;\; = \;\; v(t_0 + \Delta t/2) + a(t_0 + \Delta t)\frac{\Delta t}{2}$$

This version provides more time resolution to our calculation; however, it increases the number of calculations needed by about 50%.

1.3.2. Runge Kutta

The Runge-Kutta methods, named after the German mathematicians Carl Runge and Martin Wilhelm Kutta, family of numerical methods used to solve ordinary differential equations (ODEs) that are in the following form

$$\frac{\partial y}{\partial x} = f(x, y) \tag{1.19}$$

The basic idea behind the Runge-Kutta method is to approximate the solution of an ODE by taking small steps and using a weighted average of function evaluations at different points within each step.

$$y_{n+1} = y_n + \delta x \sum_{i=1}^{m} b_i k_i \qquad x_{n+1} = x_n + \delta x \tag{1.20}$$

where

$$k_i = f(x_n + c_i \delta x, y_n + \delta x \sum_{j=1}^{i-1} a_{ij} k_j) \tag{1.21}$$

These *equations 1.20 and 1.21* define the family of methods. To specify a pertic-

ular method, order m, coefficients a_{ij}, b_i and c_i should be provided. The coefficients of any Runge-Kutta method can be visualized by a tableau called *Butcher Tableau*.

$$
\begin{array}{c|ccccc}
0 & & & & & \\
c_1 & a_{21} & & & & \\
c_2 & a_{31} & a_{32} & & & \\
\vdots & & & \cdots & & \\
c_m & a_{m1} & a_{m2} & \cdots & a_{m,m-1} \\
\hline
& b_1 & b_2 & \cdots & b_m
\end{array}
$$

Figure 1.13: Butcher Tableau

The simplest Runge-Kutta method is the *Euler's method*. Its *Butcher tableau* is as follows.

$$
\begin{array}{c|c}
0 & \\
\hline
& 1
\end{array}
$$

The most commonly used version of the Runge-Kutta method is the fourth-order Runge-Kutta method, also known as RK4. The RK4 method involves four function evaluations per step and has an error term that is proportional to the step size raised to the fifth power. Two of the most used *Butcher tableaus* for *RK4* given below.

$$
\begin{array}{c|cccc}
0 & & & & \\
1/2 & 1/2 & & & \\
1/2 & 0 & 1/2 & & \\
1 & 0 & 0 & 1 & \\
\hline
& 1/6 & 1/3 & 1/3 & 1/6
\end{array}
\qquad
\begin{array}{c|cccc}
0 & & & & \\
1/3 & 1/3 & & & \\
2/3 & -1/3 & 1 & & \\
1 & 1 & -1 & 1 & \\
\hline
& 1/8 & 3/8 & 3/8 & 1/8
\end{array}
$$

Figure 1.14: Butcher Tableau for RK4

The second tableau in *figure 1.14* is called the *"3/8 rule"*. Its main advantage is that its error coefficients are smaller than the other. But it costs more floating point operations per step. Resulting in slower calculations.

1.4. Simulation

A simulation software is a computer program or tool that enables the creation and execution of simulations to model and analyze real-world systems or processes. It allows users to replicate the behavior, interactions, and outcomes of the system or process under study, providing insights and predictions that can be valuable for decision-making, optimization, or understanding complex phenomena.

Simulation software provides a virtual environment where users can define the parameters, variables, and rules of the system being simulated. The software then uses mathematical and physical models, algorithms, and computational techniques to simulate the behavior of the system over time.

1.4.1. Basic Consepts in Programming

1.4.1.1. Clock Cycle. In programming, a clock cycle refers to a fundamental unit of time measurement used in computer systems. It represents the basic rhythm or timing mechanism of a computer's central processing unit (CPU) and is typically measured in terms of the CPU's clock speed, expressed in hertz (Hz).

A clock cycle represents one complete pulse or oscillation of the CPU's clock signal. It serves as a synchronization mechanism, coordinating the execution of instructions and the timing of various operations within the CPU. Each clock cycle is associated with a specific duration, which is determined by the clock speed of the CPU.

The concept of clock cycles is often used when considering the performance and efficiency of algorithms and code. Since the execution time of instructions is influenced by the number of clock cycles required, minimizing the number of clock cycles needed for a program or algorithm can lead to faster and more efficient code execution. Table below shows the amount of clock cycles required for some mathematical calculations in various processors.

MEASURED CPU TIMES OF BASIC MATHEMATICAL OPERATIONS

	DOUBLE PRECISION					QUADRUPLE PRECISION	
OPERATION	i486	Pentium	PA-7000	μSPARC-II	Alpha	PA-7000	μSPARC-II
$x = y$	0.46	0.24	1.00	1.00	0.41	5.1	2.8
$x = y + z$	0.91	1.00	1.00	1.00	1.00	131	11.3
$x = yz$	1.09	1.00	1.00	1.00	1.00	457	99.5
$x = y/z$	2.81	4.49	4.92	3.32	6.59	1100	168
$x = y^{1/2}$	12.0	19.6	4.95	24.4	38.5	1100	149
$x = \sin y$	19.8	23.3	49.8	22.0	18.5	9510	1740
$x = \log y$	20.2	23.9	47.8	31.9	22.0	5420	1240
$x = \tan^{-1} y$	19.8	27.3	46.3	37.3	23.5	5930	1270
$x = \tan y$	18.0	28.3	63.2	30.0	35.1	8450	2040
$x = \exp y$	24.9	32.7	42.0	19.0	23.2	6560	1370

Figure 1.15: Amount of clock cycle for mathematical operations in various processors. [4]

Note that *division* is by far the most time consuming basic mathematical operation between addition, subtraction and multiplication.

1.4.1.2. Concurrency. Concurrency in programming refers to the ability of a program to execute multiple tasks or processes simultaneously. It allows different parts of a program to make progress independently, potentially improving performance, responsiveness, and resource utilization.

Concurrency in single core can be achieved by implementing clever scheduling of list of operations called *threads*. This results in non-blocking execution of multiple threads, but only one thread would be executed at any given time. True concurrency on the other hand, can only be achieved by using multiple cores. Each core would be able to execute one thread at any time.

Programs that implement concurrency using multiple cores executes more operations per clock cycle. However, this does not directly lead to an improved performance due to the heavy burden of scheduling and managing multiple threads.

2. DESIGN

2.1. Cavity Design

The first and the most important design parameter for a cavity is the operating RF frequency. After an operating RF frequency is set and the desired $R1/R2$ relation *figure 1.7* is selected, design parameters of acceleration plane of the cavity is fully determined.

By following the cylinderical design mentioned in *section* **??**, the only main design parameter remaining is the height of the cylindrical cavity. This parameter can be found using the constraint mentioned in *section 1.2.2*; the fact that operating RF frequency must be equal to resonant frequency of the cavity. For simple coaxial cavity, the height should be $\lambda/2$, where λ is the wavelength of the external RF supply [1]. Simulation tools such as *CST Studio, Poisson SUPERFISH* can be used to confirm this condition.

In the following examples, $p = 1$ from *figure 1.7* was used, and *it will be the focus of all further calculations.* Using $f_{RF} = 107.5$ MHz, $f_{RF} = 180$;

$$
\begin{aligned}
f_{107.5} &= 107.5 \text{ MHz} & f_{180} &= 180 \text{ MHz} \\
\lambda_{107.5} &= \frac{c}{f_{107.5}} = 2.789m & \lambda_{180} &= \frac{c}{f_{180}} = 1.666m \\
R_2 &= 0.27 \times \lambda_{107.5} = 0.753m & R_2 &= 0.27 \times \lambda_{180} = 0.450m & (2.1) \\
R_1 &= \frac{R_2}{4} = 0.188m & R_1 &= \frac{R_2}{4} = 0.113m \\
h &= \frac{\lambda}{2} = 1.394m & h &= \frac{\lambda}{2} = 0.833m
\end{aligned}
$$

In the following figures, *Poisson Superfish* and *CST* simulations of two cavities defined by *equation 2.1* can be observed.
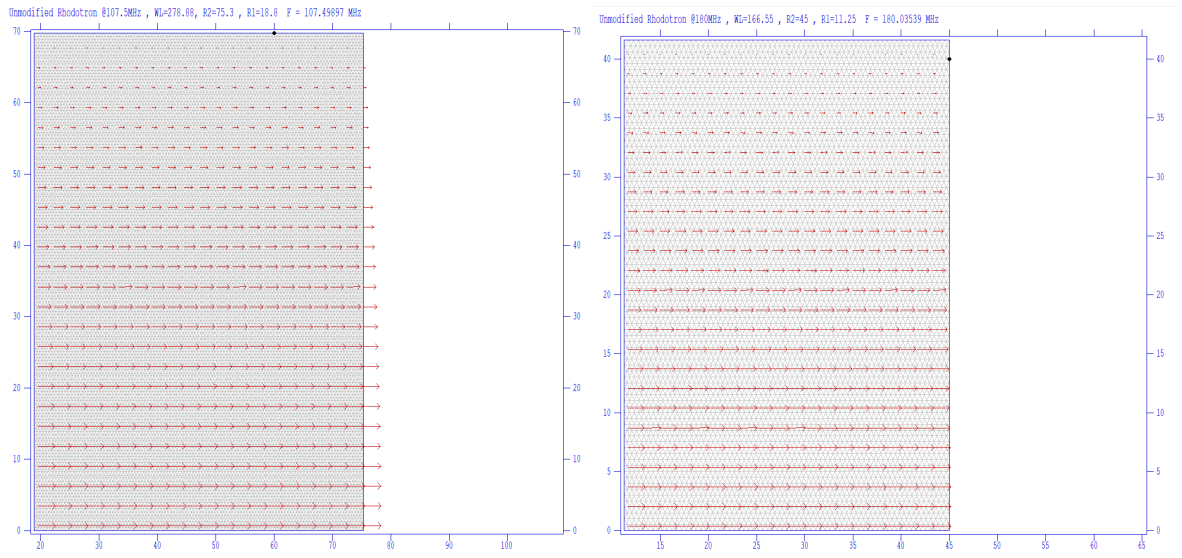
(a) 107.5 MHz

(b) 180 MHz

Figure 2.1: Poission Superfish results for *equation 2.1*
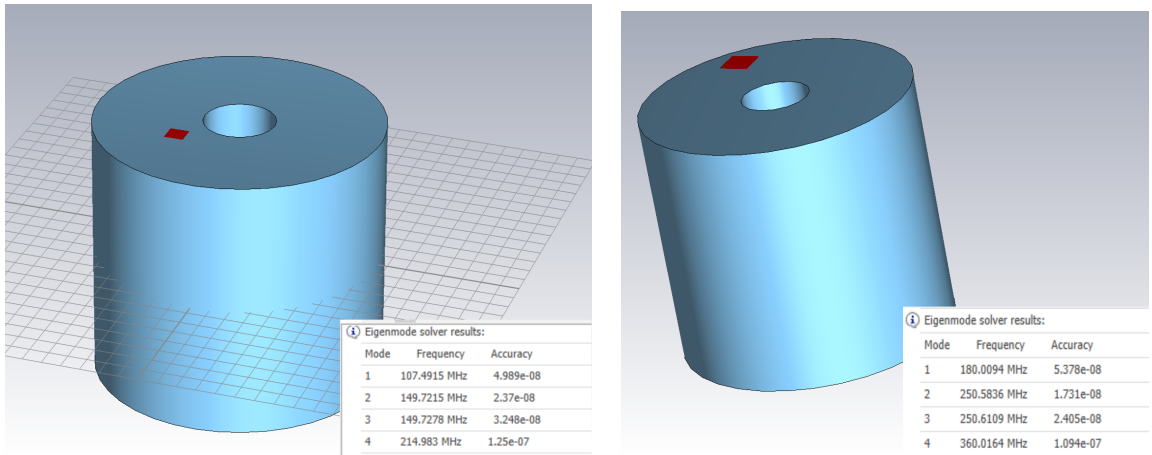
(a) 107.5 MHz

(b) 180 MHz

Figure 2.2: CST Eigenmode results for *equation 2.1*
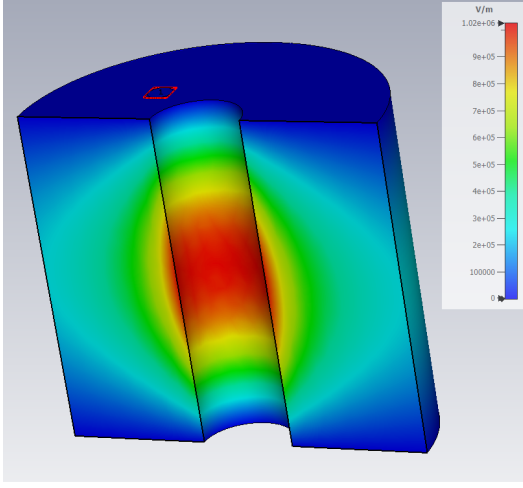
(a) 107.5 MHz
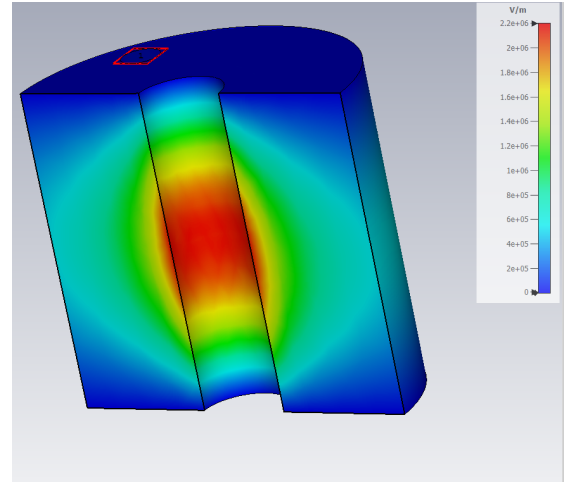
(b) 180 MHz

Figure 2.3: CST Electric field solutions for *equation 2.1*

As mentioned by POTTIER, truncated cone terminations in inner cylinder can improve the shunt empedance Z of the cavity [1]. Below, *Poission superfish* results of such a modification with matching height increase to keep resonant frequency can be found.
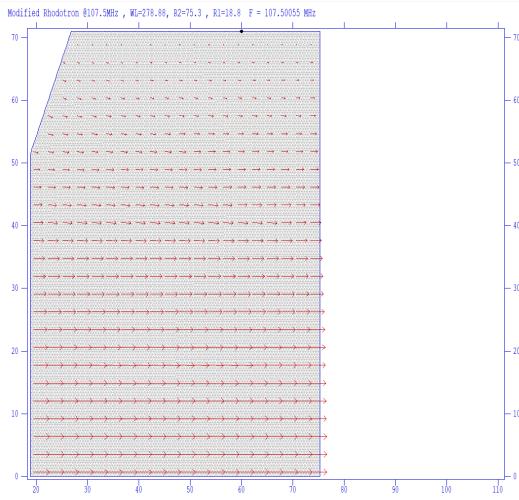
(a) 107.5 MHz truncated
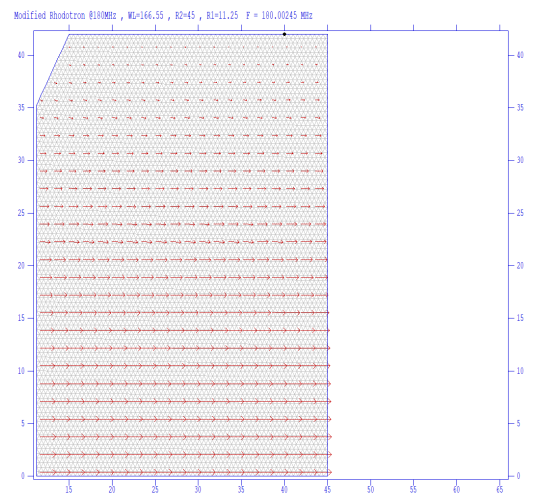
(b) 180 MHz truncated

Figure 2.4: Poisson SUPERFISH field results of truncated cavities
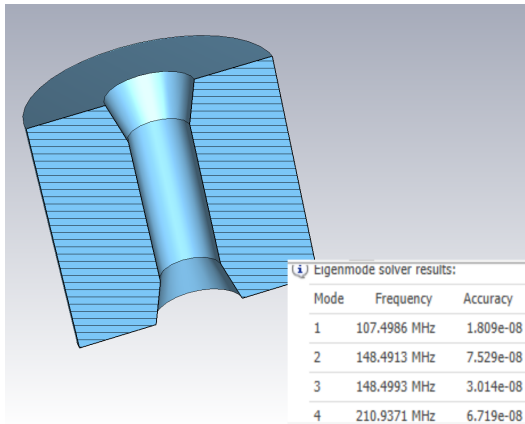
(a) 107.5 MHz truncated
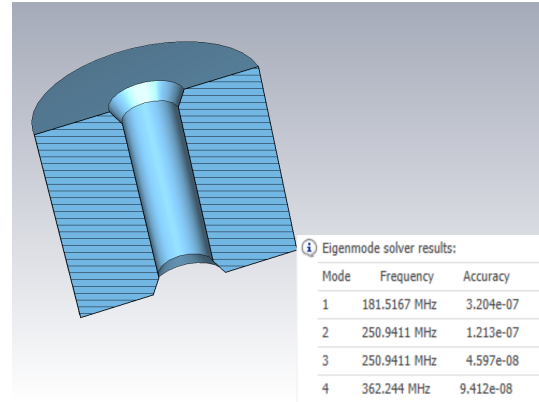
(b) 180 MHz truncated

Figure 2.5: CST eigenmode results of truncated cavities
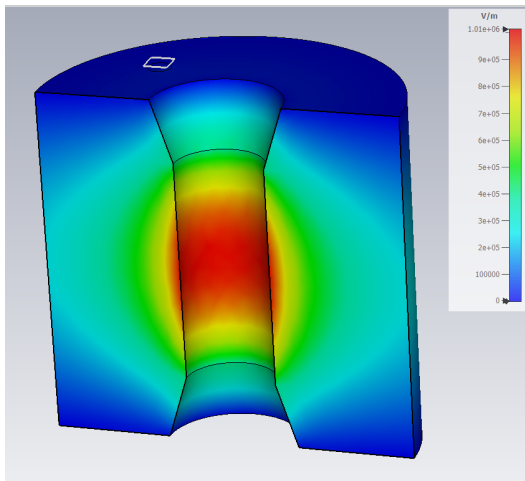
(a) 107.5 MHz truncated
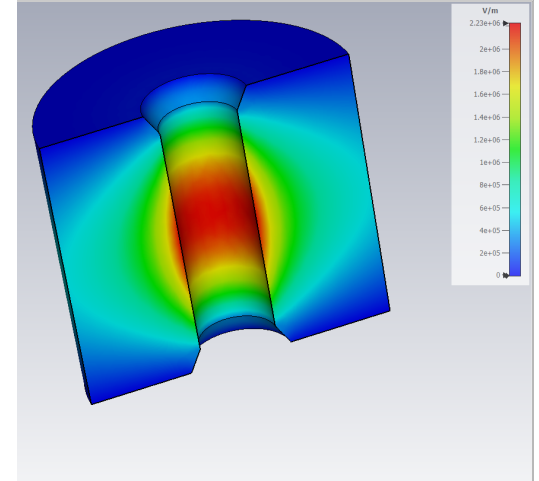
(b) 180 MHz truncated

Figure 2.6: CST electric field results of truncated cavities

(a) 107.5 MHz unmodified

(b) 180 MHz unmodified

Figure 2.7: Poisson Superfish calculations with *unmodified* cavities

```
----------------------------------------------------------------
All calculated values below refer to the mesh geometry only.
Field normalization (NORM = 0):    EZERO =     1.00000 MV/m
Frequency                              =    107.50055 MHz
Normalization factor for E0 = 1.000 MV/m =   10177.202
Stored energy                          =    0.0087482 Joules/cm
Using standard room-temperature copper.
Surface resistance                     =      2.70499 milliOhm
Normal-conductor resistivity           =      1.72410 microOhm-cm
Operating temperature                  =      20.0000 C
Power dissipation                      =     117.3652 W/cm
Q   =   50346.6        Shunt impedance =     4814.034 MOhm/m
r/Q = 54024.066 Ohm  Wake loss parameter =    9.12258 V/pC
Average magnetic field on the outer wall =   2685.64 A/m, 975.509 mW/cm^2
Maximum H (at X,Y = 73.55,71)          =     2707.68 A/m, 991.587 mW/cm^2
Maximum E (at X,Y = 75.3,0.0)          =      1.00401 MV/m, 0.086182 Kilp.
Ratio of peak fields Bmax/Emax         =       3.3890 mT/(MV/m)
Peak-to-average ratio Emax/E0          =       1.0040

Wall segments:
Segment  Xend     Yend      Emax     Power     P/A       dF/dX       dF/dY
         (cm)     (cm)      (MV/m)    (W)      (mW/cm^2)  (MHz/mm)   (MHz/mm)
------------------------------------------------------------------------
         18.800   0.0000
   1     18.800   51.400    0.9956    16.34    317.9     4.2318E-02   0.000
   2     26.800   71.000    0.3137    18.47    872.4     -4.5918E-02  -1.8742E-02
   3     75.300   71.000    4.0276E-02 47.31   975.5     0.000       -0.1350
   4     75.300   0.0000    1.004     35.25    496.4     -3.5967E-03   0.000
------------------------------------------------------------------------
                           Total     117.4
```

```
----------------------------------------------------------------
All calculated values below refer to the mesh geometry only.
Field normalization (NORM = 0):    EZERO =     1.00000 MV/m
Frequency                              =    180.00245 MHz
Normalization factor for E0 = 1.000 MV/m =   10088.517
Stored energy                          =    0.0031145 Joules/cm
Using standard room-temperature copper.
Surface resistance                     =      3.50026 milliOhm
Normal-conductor resistivity           =      1.72410 microOhm-cm
Operating temperature                  =      20.0000 C
Power dissipation                      =      90.5379 W/cm
Q   =   38905.8        Shunt impedance =     3727.719 MOhm/m
r/Q = 32337.180 Ohm  Wake loss parameter =    9.14325 V/pC
Average magnetic field on the outer wall =   2665.56 A/m, 1.24351 W/cm^2
Maximum H (at X,Y = 43.5,42)           =     2678.17 A/m, 1.2553 W/cm^2
Maximum E (at X,Y = 45,0.0)            =      1.00154 MV/m, 0.070842 Kilp.
Ratio of peak fields Bmax/Emax         =       3.3603 mT/(MV/m)
Peak-to-average ratio Emax/E0          =       1.0015

Wall segments:
Segment  Xend     Yend      Emax      Power    P/A       dF/dX       dF/dY
         (cm)     (cm)      (MV/m)    (W)      (W/cm^2)  (MHz/mm)   (MHz/mm)
------------------------------------------------------------------------
         11.250   0.0000
   1     11.250   35.250    0.9981    17.74    0.5033    7.6469E-02   0.000
   2     15.000   42.000    0.1761    9.122    1.181     -8.1176E-02  -4.5098E-02
   3     45.000   42.000    3.1924E-02 37.29   1.243     0.000       -0.3870
   4     45.000   0.0000    1.002     26.38    0.6282    -4.6971E-03   0.000
------------------------------------------------------------------------
                           Total     90.54
```

(a) 107.5 MHz truncated   (b) 180 MHz truncated

Figure 2.8: Poisson Superfish calculations with *truncated* cavities

One can observe the shunt impedance gain between truncated and unmodified cavities in *figures 2.7 and 2.8*;

$$\Delta Z_{107.5} = 2.5\% \qquad \Delta Z_{180} = 2.7\%$$

2.2. Magnet Design

Magnet design in rhodotron type accelerators depend heavily on the design of the cavities. Because the limiting factors usually are frequency and total volume of the accelerator, magnet design parameters are considered after cavity design has been completed. Considering the nature of coaxial cavity, simplest path for beams inside magnets is major segment of a circle, which was used as the reference for following discussions.
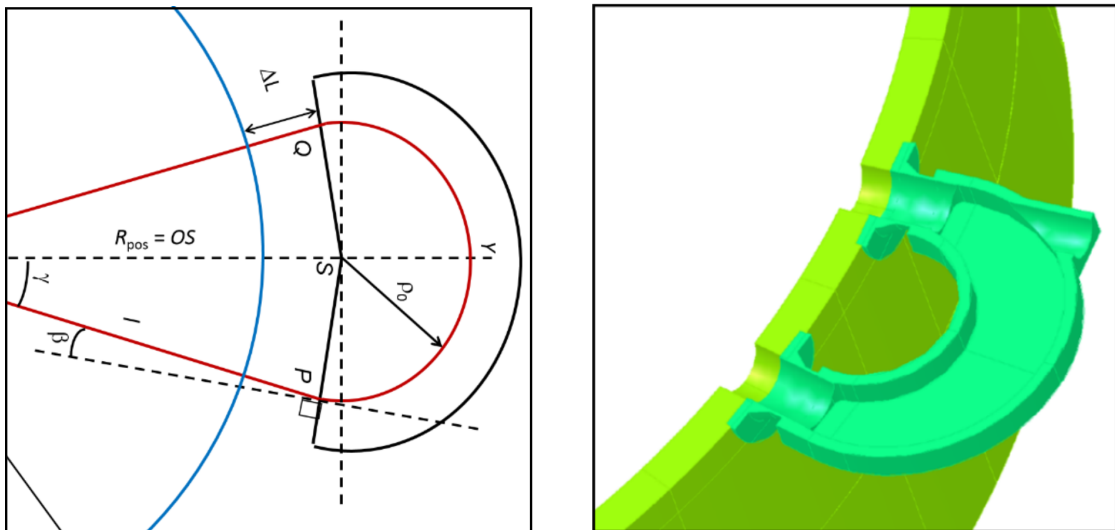
(a) Geometry of the outside trajectory
of a rhodotron [5]

(b) Modeling of the outside trajectory
of a rhodotron (TT300) [5]

Figure 2.9: From "Design and Simulation Tools for the
High-Intensity Industrial Rhodotron Electron Accelerator,"
by W.Kleeven, M.Abs, J.Brison, E.Forton, J.Hubert and J.Van de Walle

In rhodotron accelerators, magnets are used for not only guiding the electron beam to desired path, but also for syncronizing them with the RF field in the cavity. This syncronization, also called phase stability, is the fundamental constraint of magnet design. Time spent outside of the cavity should be precisely tuned to maximize acceleration in the succeeding pass.

Two different approaches have been used to achieve phase stability. These ap-

proaches are discussed further in the following sections.

2.2.1. $n\lambda$ Technique

First approach for phase stability considiration assumes that from the start of the current pass, $\beta_{avg} \approx 1$ for a synchronous particle.

To maintain the phase synchronization, a particle that started the current pass at $t = 0$, should start the next pass at $t = nT$, where n is an integer and T is the period of RF field inside cavity. As discussed earlier, by assuming the electron is traveling at c, phase stability can be achieved by designing the whole trajectory to be $n\lambda$, where λ is the wavelength of the RF field. In other words, total trajectory of synchronous particle needs to satisfy the following equality;

$$L_{pass} = n\lambda$$

Since $n > 1$ would require unnecessarily long and expensive beam guide and magnets, $n = 1$ is the most efficient choice.

$$L_{pass} = \lambda \tag{2.2}$$
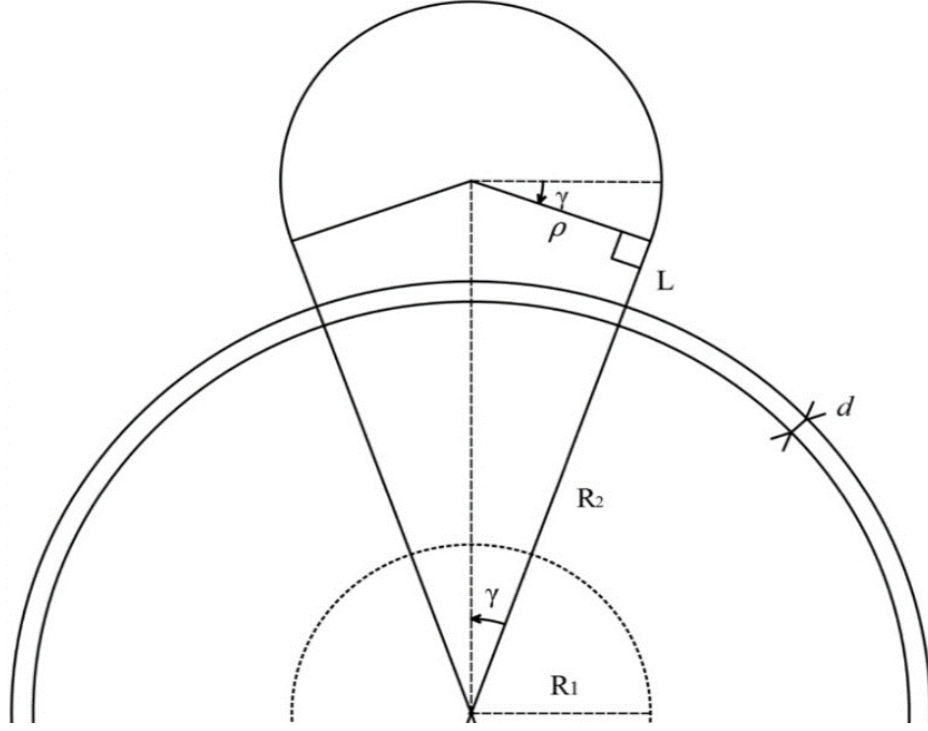
Figure 2.10: Trejectory of a particle in single pass

From *figure 2.10*, where γ is half the angle between trajectories of successive passes, ρ is the radius of the circular path inside magnet, L is the length of the magnet guide, d is the thickness of the cavity wall;

$$
\begin{aligned}
L_{in} &= 2R_2 \\
L_{out} &= 2L + 2d + (\pi + 2\gamma)\rho \\
L_{pass} &= L_{in} + L_{out} \\
\lambda &= 2R_2 + 2d + 2L + (\pi + 2\gamma)\rho
\end{aligned}
\tag{2.3}
$$

After the cavity design is complete, only L, γ and ρ remain, which are the design parameters of magnets. Observing the *figure 2.10* and using *equation 2.3,*

$$\begin{aligned}
tan(\gamma) &= \frac{\rho}{R_2 + d + L} \\
\rho &= tan(\gamma)(R_2 + d + L) \\
2\rho &= tan(\gamma)(\lambda - (\pi + 2\gamma)\rho) \\
\rho(2 + tan(\gamma)(\pi + 2\gamma)) &= tan(\gamma)\lambda \\
\rho &= \frac{\lambda}{\pi + 2\gamma + \frac{2}{tan(\gamma)}} \quad (2.4) \\
L + d &= \frac{\rho}{tan(\gamma)} - R_2 \quad (2.5)
\end{aligned}$$

Equations 2.4 and 2.5 define 2 constraints. As already discussed, it has been assumed that cavity design is set (*i.e* R_2, λ, d are already defined). Therefore only the magnet design parameters ρ, γ and L are left. Together with the constraints, one free variable defines the whole magnet design. Considering the importance of γ for maximum number of possible passes, it will be used as the free magnet design variable in the further discussions.

2.2.2. L_{out} Parameter Sweep

As mentioned previously in *section 2.2.1*, *equation 2.3* assumes that the particles are fast enough so that $\Delta t_{pass} \approx nT$. This assumption is not guaranteed however, especially in the first few passes if the particles are not accelerated enough. This scenario can happen when RF power is not sufficiently high.

Consider an RF supply with $f = 1$ GHz, $P = 50$ kW. Using *equation 1.14*, after the first pass the synchronous electron that entered the accelerator with 40 keV and $\phi = 15°$ phase lag,

$$\begin{aligned}
W_{gain} &= 2.14 \times 0.2998^{1/4} \times 50000^{1/2} = 354 keV \\
W_{total} &= 394 keV
\end{aligned}$$

$$\beta_{40keV} \approx 0.374$$
$$\beta_{394keV} \approx 0.825$$

It is clear that β_{avg} is not fast enough to sustain phase stability if the magnet is designed for $\beta = 1$. For these cases, *equation 2.3* fails to deliver phase stability. Another approach for designing a magnet would be to find a new constraint, K for total path length.

$$L_{pass} = K$$
$$L_{in} + L_{out} = K$$

Since L_{in} is set previously from cavity design, we can remove it from our equation and continue with

$$L_{out} = K \tag{2.6}$$

To start, an optimization criteria for the following pass such as

- Ensure the phase stability of the synchronous electron
- Maximize the energy gain of the synchronous electron
- Minimize the energy spread of the beam
- Minimize the phase lag spread of the beam
- All of the above with decided weights

needs be selected. Using a simulation software such as *CST Studio Particle Module*, the optimum value of K for the criteria can be found by simulating for different values of K (*sweeping*) and analyzing the results. This process can be repeated for each magnet until the desired beam characteristics in the end of the accelerator are achieved.

However, one caviat of this technique is that, available simulation softwares are not well suited for this kind of process. As mentioned above, *CST Studio Particle Module* has a *parameter sweep* functionality. But the calculation times are too slow to be useful in this particular problem. *A custom built software offering magnet optimizing sweep functionality will be discussed in the following chapter.*

2.3. Initial Design at KAHVELab

A rhodotron with operation frequency of 107.5 MHz was decided to be built at KAHVELab. After considering the earlier simulations mentioned in *sections 2.1 and 2.2*, an initial design was created.
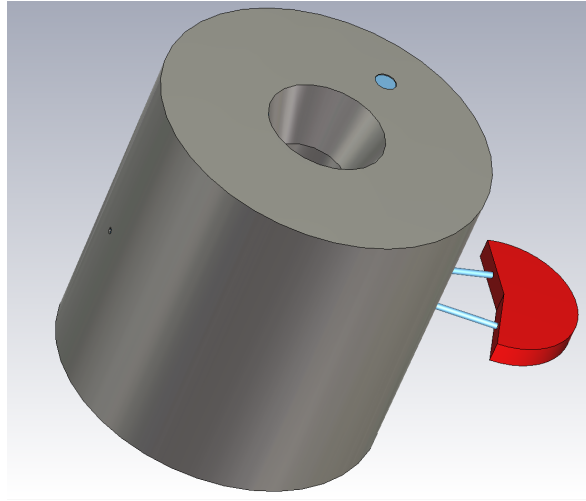
Figure 2.11: Initial design of the proposed rhodotron

$$\gamma = 9°$$
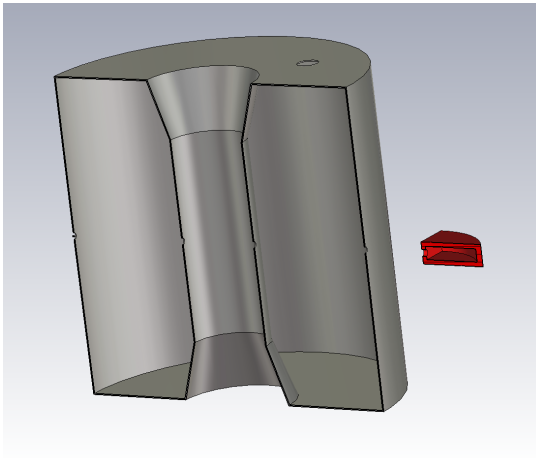
(a) Axial cross section.
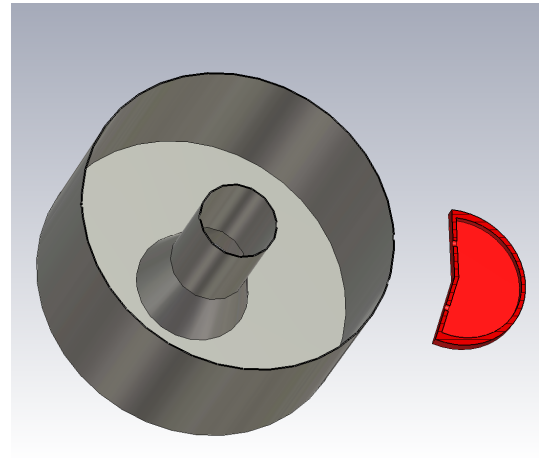
(b) Cross section at acceleration plane.

Figure 2.12: Initial design of the proposed rhodotron.

The magnets used in this design is the simplest in terms of design parameters. It consists of an iron casing encapsulating the shape of desired magnetic field, which are

created by two coils inside.
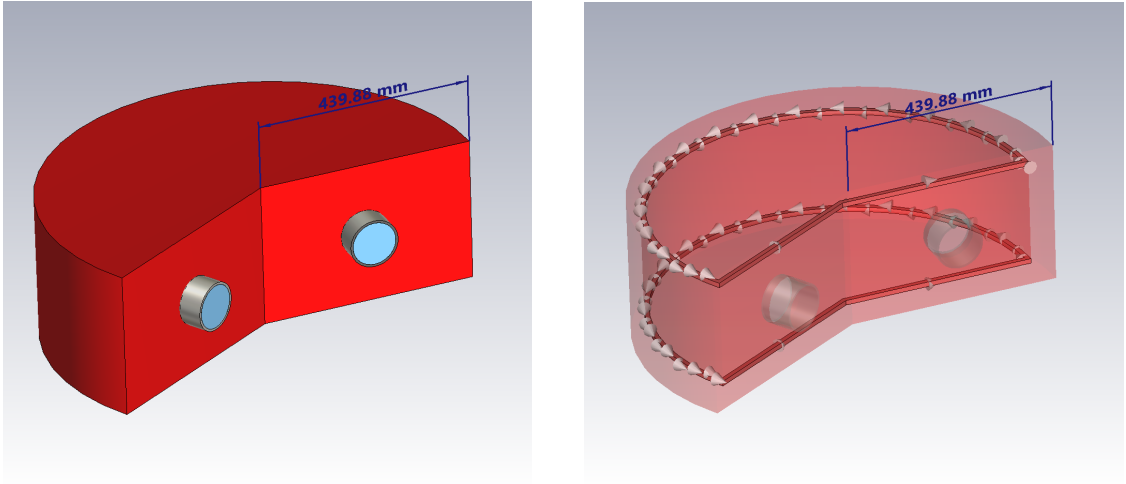
Figure 2.13: Initial magnet design.
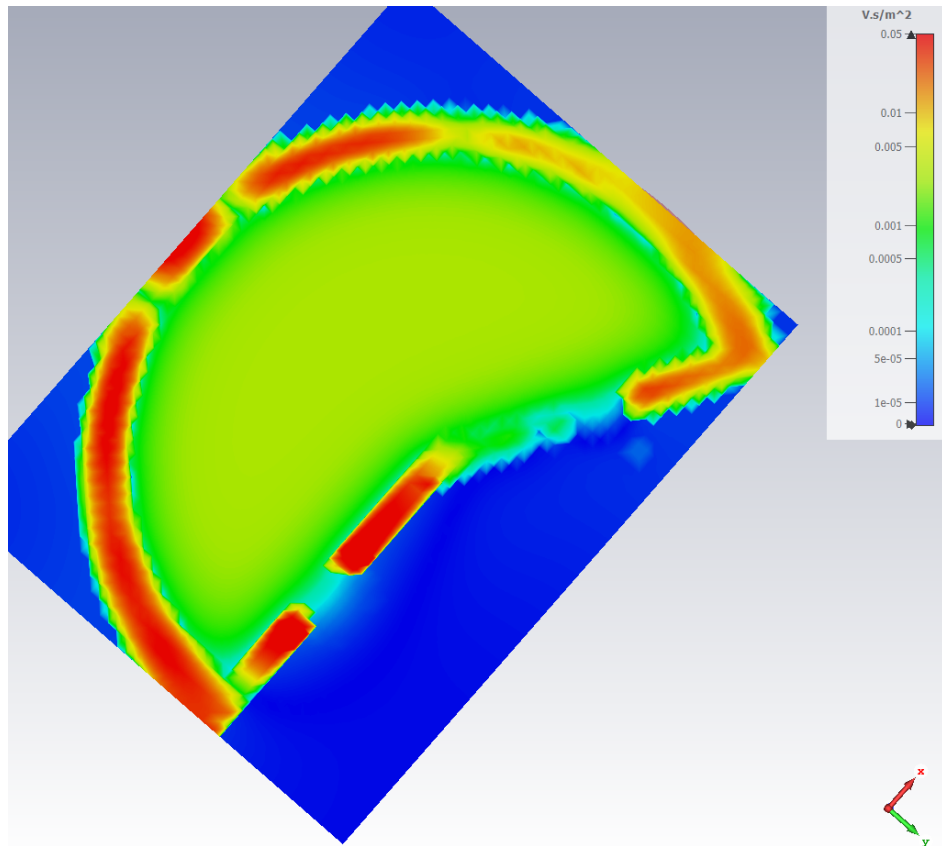
Figure 2.14: Magnetic field in acceleration plate of initial magnet design.

figure 2.14 shows that this design provides relatively uniform magnetic field inside, although magnetic field gradient in the openings can be improved.

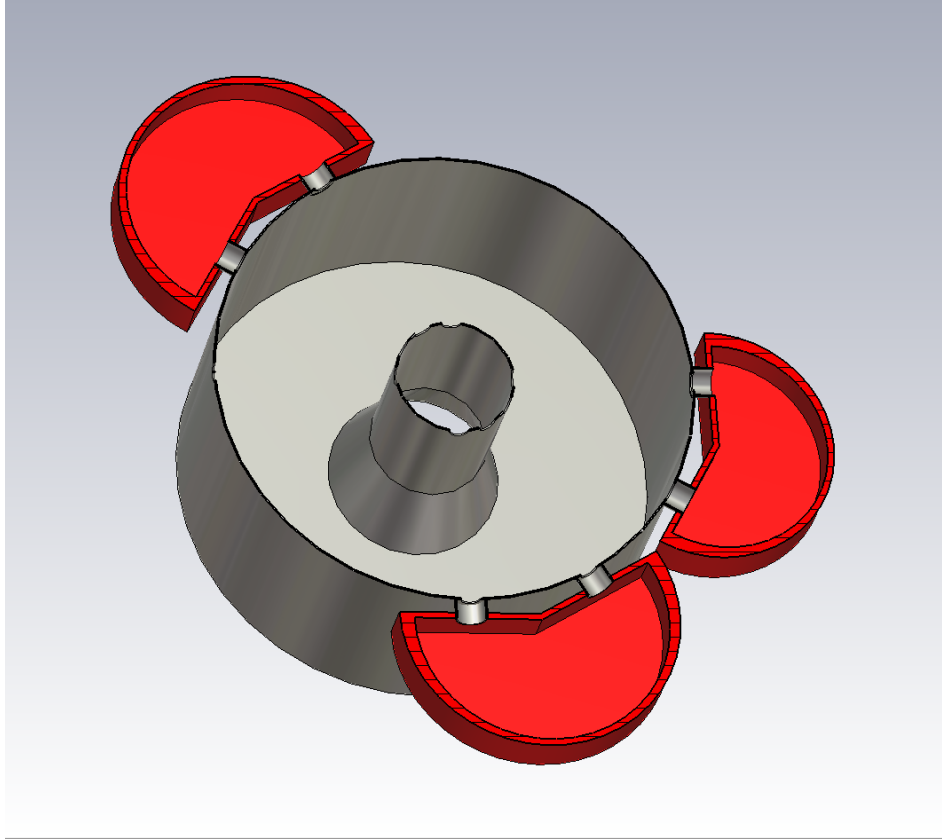After adding two more magnets and using $\gamma = 15°$, the following second prototype design was created

Figure 2.15: Initial cavity with three magnets as shown in *figure 2.13*
$\gamma = 15°$

These designs, together with 40 keV e^- gun injecting with phase lag of 15° for 0.1 ns, was simulated at RF power of 50 kW using *CST Studio Particle Module PIC Solver*. Results of these simulations can be found in *figure 2.16*.
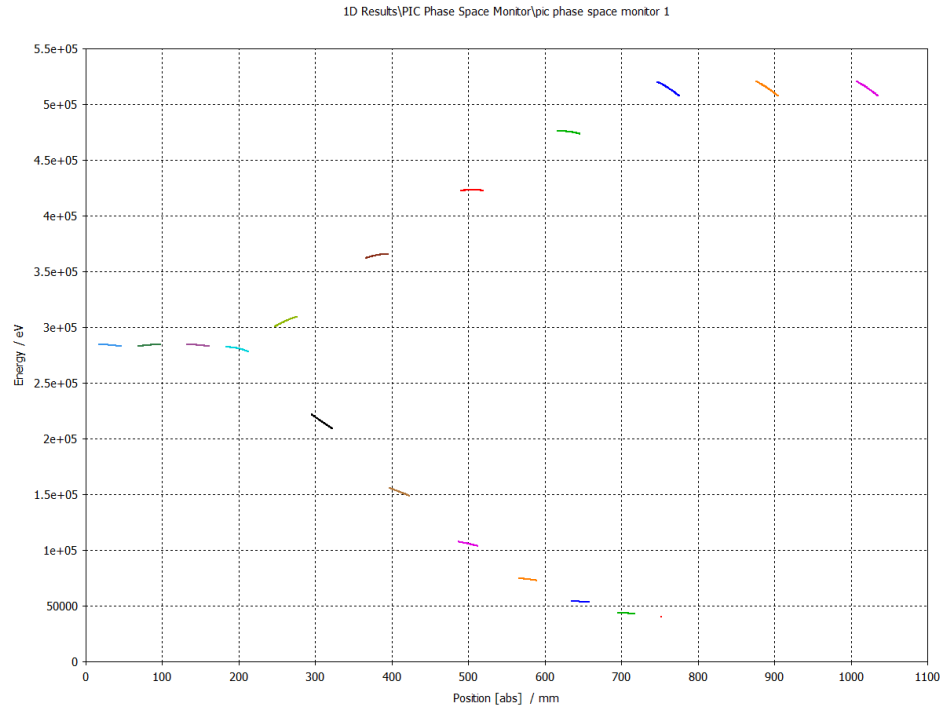
(a) One pass simulation of *figure 2.11*
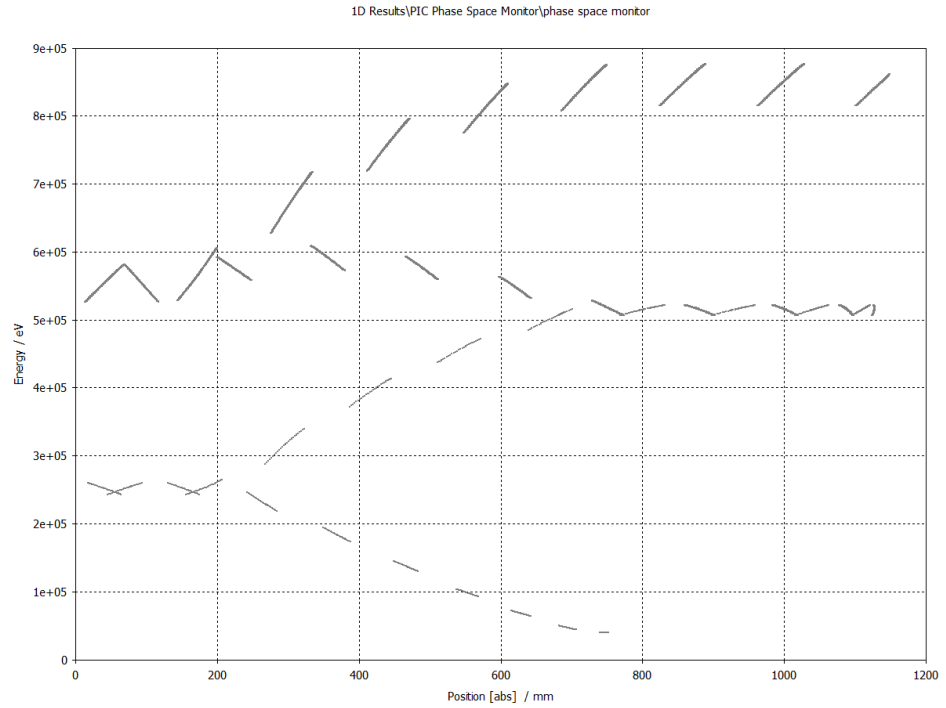
(b) Two pass simulation of *figure 2.15*

Figure 2.16: $|r|$ vs *Energy* simulation of initial design.

The behavior of the beam in the *figure 2.16* after the first pass indicates that phase stability is not maintained. When the simulation results are examined further, it was observed that the beam started the second pass at $t \approx 12$ ns after the injection. Considering the starting phase lag $\phi_{lag} = 15°$, this would mean phase lag of the second pass was $\phi_{lag2} = 120°$. This result can be observed in *figure 2.16*, as the beam decelerates after a short acceleration in the beginning of the second pass.

After various similar observations in *CST* similations, underlying cause of this problem was thought to be the $L_{pass} = n\lambda$ approach on magnet design failing in low energies, as anticipated and discussed earlier in the *section 2.2.2. The necessity for an alternative tool, capable of aiding researchers in improving beam behavior, was deemed evident.*

In KAHVELab, several improvements were made to these initial designs by *Mr. Sinan ÖZ.* They include curved edges on cavity which reduce the power loss on cavity walls, and redesigned iron casing on magnets for ease of production and maintenance. Improved designs can be seen in the figures below.
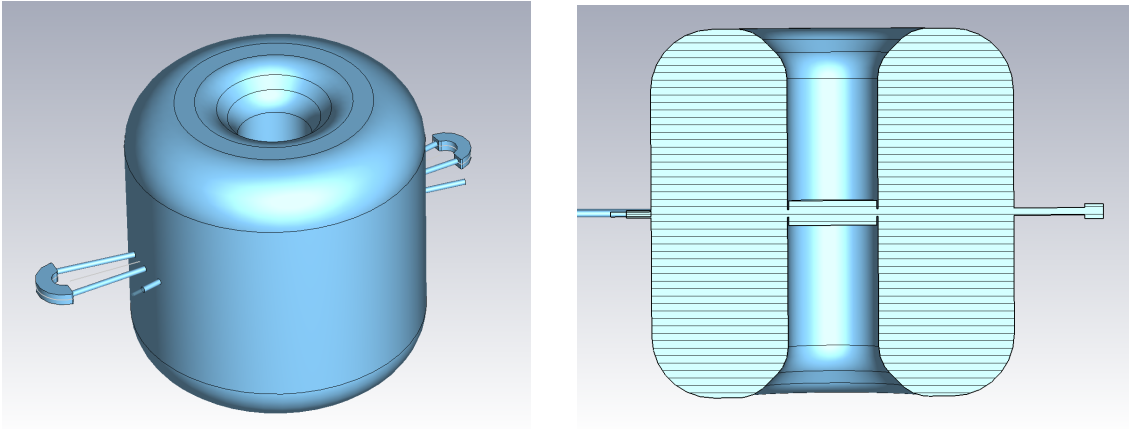

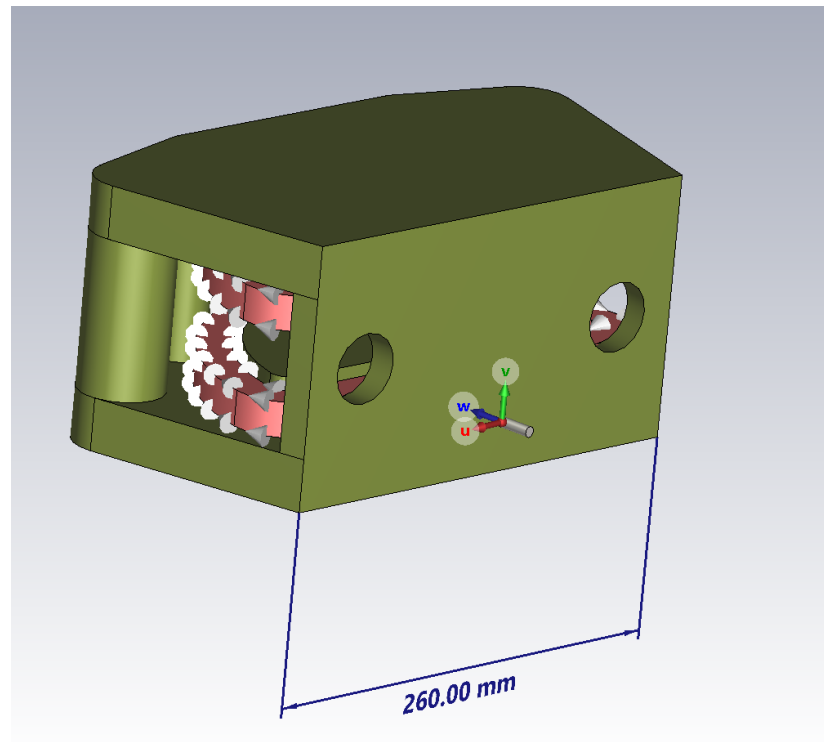Figure 2.17: Improved cavity design.
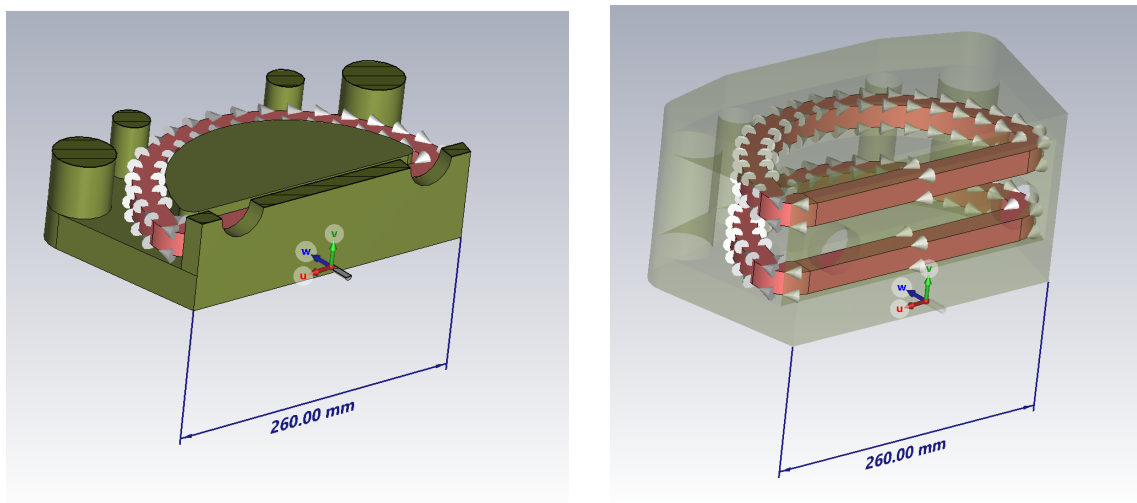
Figure 2.18: Improved magnet design.

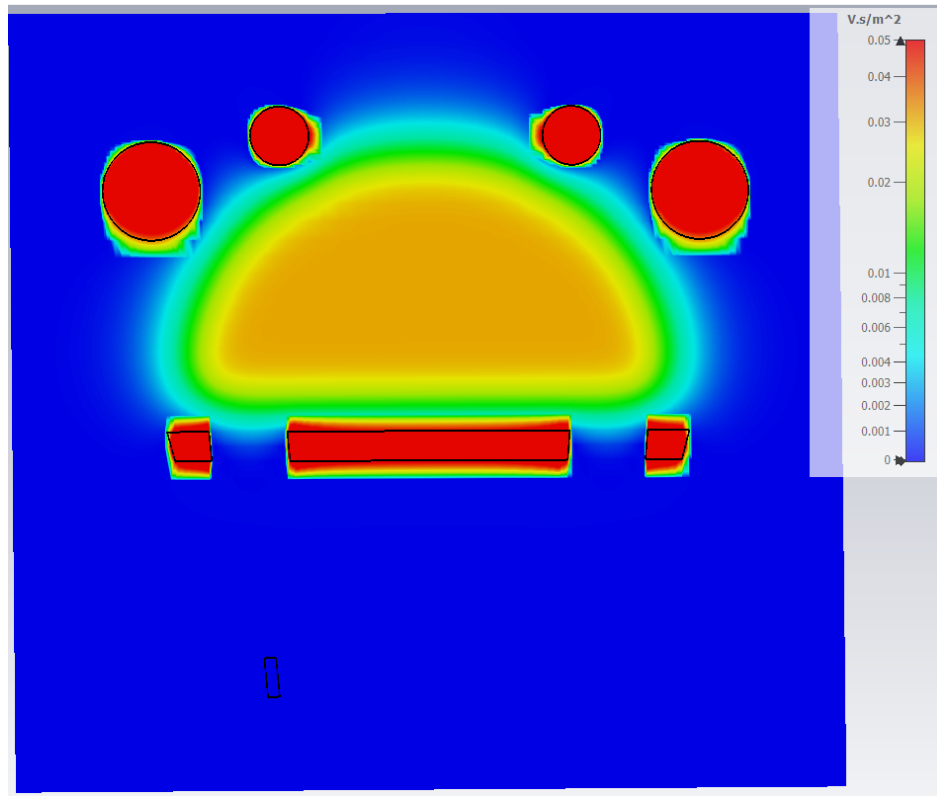Figure 2.19: Cross section and coils of improved magnet design.

Figure 2.20: Magnetic field in acceleration plate of improved magnet design.

From *figures 2.14 and 2.20*, it can be observed that improved magnet design reduces magnetic field leak in enter and exit openings considerably. This reduction helps containing the spread of entering beam, decreasing the amount of focusing needed further into trajectory.

REFERENCES

1. Jacques Pottier, *A new type of rf electron accelerator: The rhodotron*, Nuclear Instruments and Methods in Physics Research Section B: Beam Interactions with Materials and Atoms, Volumes 40–41, Part 2, 1989, Pages 943-945,

2. J.M. Bassaler, J.M. Capdevila, O. Gal, F. Lainé, A. Nguyen, J.P. Nicolaï, K. Umiastowski, *Rhodotron: an accelerator for industrial irradiation*, Nuclear Instruments and Methods in Physics Research Section B: Beam Interactions with Materials and Atoms, Volume 68, Issues 1–4, 1992, Pages 92-95,A:

3. Y. Jongen. (2001). *Manufacturing of Electron Accelerators*. Ion Beam Applications s.a. (IBA) Chemin du Cyclotron 3, B-1348 Louvain-la-Neuve, Belgium.

4. Fukushima, Toshio. (2001). *Reduction of Round-off Errors in Symplectic Integrators*. The Astronomical Journal. 121. 1768-1775.

5. W. Kleeven, M. Abs, J. Brison, E. Forton, J. Hubert and J. Van de Walle, *Design and Simulation Tools for the High-Intensity Industrial Rhodotron Electron Accelerator*, 9th International Particle Accelerator Conference, 2018